Sparse ICA for Blind Separation of Transmitted and Reflected Images

Alexander M. Bronstein,[1] Michael M. Bronstein,[1] Michael Zibulevsky,[2] Yehoshua Y. Zeevi[2]

[1] Department of Computer Science, Technion – Israel Institute of Technology, Haifa 32000, Israel

[2] Department of Electrical Engineering, Technion – Israel Institute of Technology, Haifa 32000, Israel

Received 17 November 2004; accepted 25 January 2005

ABSTRACT: We address the problem of recovering a scene recorded through a semireflecting medium (i.e. planar lens), with a virtual reflected image being superimposed on the image of the scene transmitted through the semirefelecting lens. Recent studies propose imaging through a linear polarizer at several orientations to estimate the reflected and the transmitted components in the scene. In this study we extend the sparse ICA (SPICA) technique and apply it to the problem of separating the image of the scene without having any a priori knowledge about its structure or statistics. Recent novel advances in the SPICA approach are discussed. Simulation and experimental results demonstrate the efficacy of the proposed methods. © 2005 Wiley Periodicals, Inc. Int J Imaging Syst Technol, 15, 84–91, 2005; Published online in Wiley InterScience (www.interscience.wiley.com). DOI 10.1002/ima.20042

Key words: transparent layers; reflection; polarization; sparseness; ICA; blind source separation (BSS); wavelet packets; clustering

I. INTRODUCTION

The phenomenon of a virtual image being semireflected by a transparent medium, situated along the optical axis somewhere between the imaged scene and the observing point, and superimposed on the imaged scene, is typical of many optical setups. It may arise, for example, when photographing objects situated behind a glass window or windshield, since most types of glass have semireflecting properties. The need to separate the contributions of the real and the virtual images to the combined, superimposed, images is important in applications where reflections may create ambiguity in scene analysis. Separation of the desired image from the superimposed reflection is of particular importance in systems implementing vision algorithms based on feature matching. Also, since the virtual and the real images may appear at different distances from the camera, the reflections may confuse autofocusing devices (Schechner et al., 1999, 2000).

Approaches to reconstruction of the virtual and the real images, based on polarimetric imaging, have attracted attention during the last few years (Cronin et al., 1994; Nayar et al., 1997). Incorporation of a polarizer into the optical system is a common photographic technique allowing suppression of semireflective layers (Schechner et al., 1999, 2000). Several constructions of such cameras, e.g., a system equipped with a liquid crystal polarizer (Fujikake et al., 1998), were recently proposed.

However, the polarizer is capable of removing the reflected component completely only when the viewing angle is equal to the Brewster angle. This case results, however, in severe geometric distortions. In other cases, the polarization is not sufficient (Farid et al., 1999a; Schechner et al., 1999, 2000); even when the polarizer is oriented to minimize the reflected component, the virtual image is still visible (Fig. 1b).

Several signal postprocessing approaches were proposed in recent studies; however, they rely mainly on motion, stereo, and focus, and assume that the real and the virtual objects lie at significantly different distances from the camera (Bergen et al., 1990; Shizawa, 1992). Other methods assume some knowledge about the scene, such as the semireflector angle and refraction index, which makes them hardly feasible in the general case (Schechner et al., 1999, 2000).

Farid and Adelson (1999a,b) apply an analytic version of independent component analysis (ICA) for blindly separating the reflected and the transmitted images. Such an approach does not require any prior knowledge regarding model parameters, and offers better feasibility in real-world applications. However, the proposed method is not general enough, since it works with two sources only. On the other hand, iterative approaches such as the information maximization (Infomax) algorithm (Bell and Sejnowski, 1995) are relatively slow, although they can handle any number of sources, provided a sufficient number of mixtures are available.

It has been recently demonstrated by Zibulevsky and Pearlmutter (2001), Zibulevsky et al. (2001b), and by Kisilev et al. (2000, 2003) that sparseness can significantly improve the accuracy and the computational efficiency of existing ICA algorithms. In addition, sparse decomposition allows using simple "geometric" algorithms to separate the mixed data. We adopt the sparse ICA

Correspondence to: Michael Zibulevsky; e-mail: mzib@ee.technion.ac.il

© 2005 Wiley Periodicals, Inc.

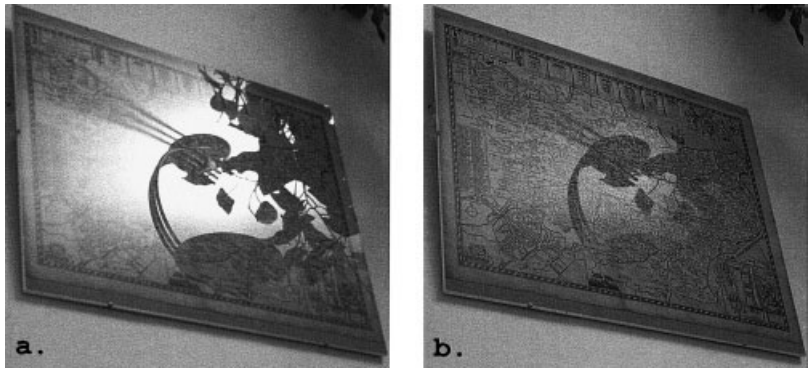


Figure 1. The effect of polarization imaging on reflection removal. A glass-framed picture was photographed through a polarizer, set in a position to maximize (a) and to minimize (b) the reflected component. Note that even when the reflection is minimized, the virtual image is still clearly visible.

(SPICA) approach and show that it affords effective separation of a transmitted image from superimposed reflections.

We first formulate in Section II the problem of removal of semireflected images as a linear blind source separation (BSS) problem, and then proceed to discuss in Section III the motivation for utilizing sparse representations for the purpose of BSS. This leads to the presentation of the SPICA method. Section IV is devoted to the question of how to obtain a sparse decomposition of images in order to exploit the advantages of the sparseness. We introduce several new approaches, suitable for decomposition of natural images. In Section V, we apply the algorithm to simulated and real-world images and compare it with the previously proposed approaches.

II. THE BSS PROBLEM

A typical optical setup involving a semireflector is shown in Figure 2. The real object (a) is situated on the optical axis behind a semireflecting planar lens (d), e.g., glass window or windshield, inclined with respect to the optical axis (Schechner et al., 1999, 2000). Another object (b) is partially reflected by the lens, creating a virtual image (c). The camera (f) records a superposition of the two images. That is, the intensity of the observed mixture image at a single point is given by

$$m_1 = a_{11}s_1 + a_{12}s_2, \tag{1}$$

where s_1 and s_2 are the images of two source objects (a) and (b), and a_{11}, a_{12} are scene-dependent multiplicative constants, which can, in the case of a planar semireflector, be assumed invariant w.r.t. the independent spatial variables (i.e. space invariant).

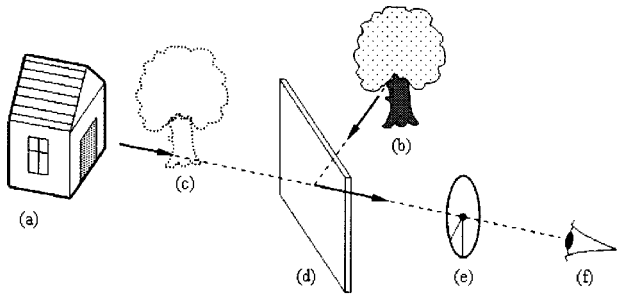


Figure 2. A typical optical setup including a semireflector: (a) object 1, (b) object 2, (c) virtual object, (d) glass, (e) polarizer, (f) camera.

Since the reflected light is polarized, by introducing a linear polarizer (e), the relative weights of the two mixed images can be varied, thus yielding mixtures of the form

$$m_n = a_{n1}s_1 + a_{n2}s_2, \quad n = 1, \ldots, N \tag{2}$$

or in matrix notation

$$\begin{pmatrix} m_1 \\ \vdots \\ m_N \end{pmatrix} \cdots = \begin{pmatrix} a_{11} \cdots & a_{12} \cdots \\ \vdots & \vdots \\ a_{N1} & a_{N2} \end{pmatrix} \cdot \begin{pmatrix} s_1 \\ s_2 \end{pmatrix}; \quad M = A \cdot S, \tag{3}$$

where $m_1, \ldots, m_n$ are the N mixed images and s_1 and s_2 are the two source images represented as row vectors, and A is the matrix that produces the linear mixtures (usually referred to as the *crosstalk* or the *mixing* matrix). The mixing matrix is usually unknown, unless there exists an exact optical model of the underlying scene. Our goal is to determine the two source images S from the set of equations (3) with an unknown mixing matrix. Such a problem is usually referred to as the BSS problem. Under the assumption that the sources are statistically independent (which is reasonable in the presented case), it is possible to recover sources s_1 and s_2 up to a permutation and multiplicative constant, by estimating the mixing matrix $\tilde{A} \approx A$, and estimating the sources by means of the inverse

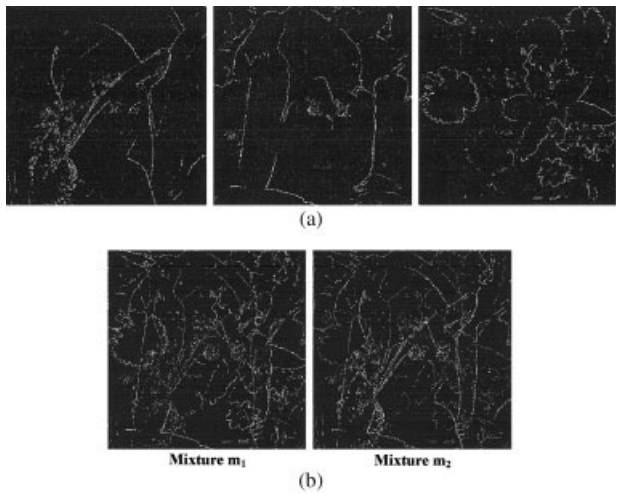


Figure 3. Three sparse images containing about 5% of nonzero samples and two synthetic mixtures.

10981098, 2005, 1, Downloaded from https://onlinelibrary.wiley.com/doi/10.1002/ima.20042 by CochraneAustria, Wiley Online Library on [23/09/2026]. See the Terms and Conditions (https://onlinelibrary.wiley.com/terms-and-conditions) on Wiley Online Library for rules of use; OA articles are governed by the applicable Creative Commons License

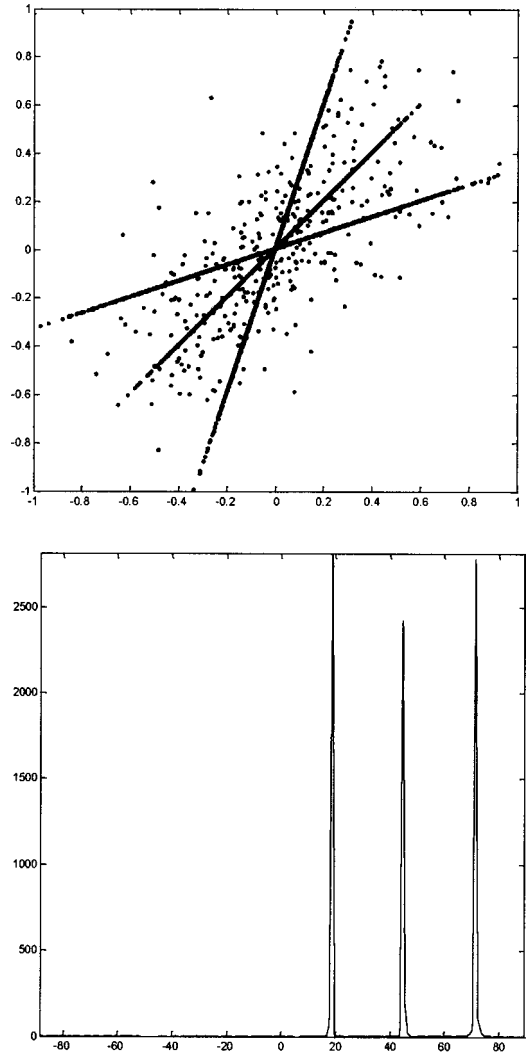


Figure 4. Scatter plot of the mixtures m_2 vs. m_1 (a) and the angular histogram of the scatter plot (b). The orientations and the peaks A–C in the histogram correspond to Sources A–C.

of $\tilde{A}$:

$$\tilde{S} = \tilde{A}^{-1} \cdot M. \tag{4}$$

The solution is possible using the SPICA method, as discussed in the sequel.

III. SPARSE ICA

The idea motivating the development of the SPICA method is based on the observation that most natural signals and images can be projected onto a space of sparse representation by the action of a proper sparsifying transformation (Zibulevsky and Pearlmutter, 2001; Zibulevsky et al., 2001b). An intuitive understanding of SPICA is guided first by considering the case of sparse sources. The approach is then extended to general nonsparse signals.

A. Separating Sparse Images. As a motivating example, we begin with a case in which the sources are sparse. Sparseness implies that only a small number of the signal samples are significantly different from zero. Three sparse source images were mixed using a random

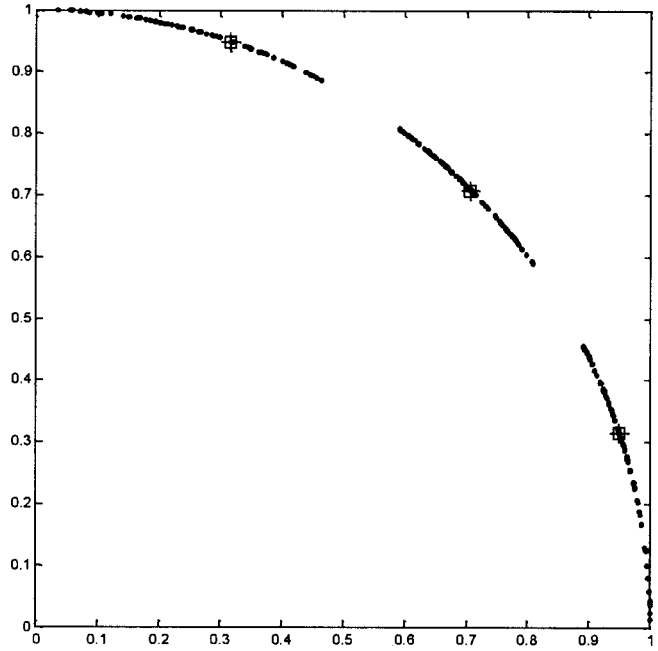


Figure 5. Coefficients' distribution after their projection onto a hemisphere and clustering with refined fuzzy C-means (FCMs). Cluster centers are marked with squares.

matrix. The sources had about 5% of nonzero samples. The location of the nonzero samples in the images was statistically independent (Fig. 3). The mixtures were adjusted to have zero mean.

Since most pixels in the source images have a near-zero magnitude and the locations of the nonzero pixels in the sources are statistically independent, there is a high probability that only a single source will contribute to a given pixel in each mixture. Consequently, the majority of the pixels in each mixture will be influenced by one source only and have a magnitude equal to that of the source multiplied by the corresponding coefficient of the mixing matrix. In



Figure 6. Two sources (A and B) and their mixed images.

10981098, 2005, 1, Downloaded from https://onlinelibrary.wiley.com/doi/10.1002/ima.20042 by CochraneAustria, Wiley Online Library on [23/09/2026]. See the Terms and Conditions (https://onlinelibrary.wiley.com/terms-and-conditions) on Wiley Online Library for rules of use; OA articles are governed by the applicable Creative Commons License

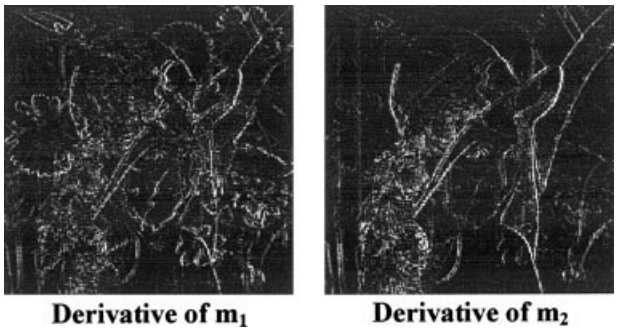


Figure 7. The transformed mixtures obtained by the action of derivative in *x*-direction.

the scatter plot of one mixture versus the other, these data will therefore cluster along lines, each corresponding to a source, at a distance from the center depending on source magnitude. It is therefore possible to estimate the ratios of sources' contribution to the mixtures by measuring the angles of the centroids of the colinear clusters.

Figure 4a depicts a scatter plot of the mixtures. The colinear clusters identifying the columns of the mixing matrix are clearly visible, so that one can estimate the angles (e.g., from the angular histogram, Fig. 4b) and thereby the matrix entries. This observation highlights our approach to the development of the separation algorithms, which we address as being *geometric* and present it in Section III.B.

B. Geometric Separation. Geometric separation approaches are based on the detection of colinearities in the distribution of the coefficients over the scatter plot. The straightforward way to estimate the proper orientations with reference to the scatter plot is by using the angular histogram. Applications of this approach are limited to low dimensions (practically to 2D) because of the difficulty in constructing the angular histogram in higher dimensions. The M points in the scatter plot (M equals the number of pixels in the image) are represented as points in N-dimensional space (in our case, $N = 2$). Since the mixtures are assumed to have a zero mean, the oriented colinear distributions are centered at the origin. For each point $c_k \in \mathbb{R}^2$, the angle

$$\alpha_k = \tan^{-1}\left(\frac{c_k^2}{c_k^1}\right) \tag{5}$$

is computed. Constructing the histogram of α, it is possible to detect the optimal orientations using a peak-detection algorithm. In case of two sources and two mixtures ($K = N = 2$), the histogram has a bimodal shape. Hence, fitting with two Gaussians (*bimodal fitting*) can be used for peak detection.

An alternative approach of data clustering along orientations in the scatter plot is as follows: each point $\boldsymbol{c}_k$ is projected on a unit hemisphere, by normalizing the data vectors:

$$\boldsymbol{c}_k = \frac{c_k}{\|c_k\|} \tag{6}$$

and multiplying them by the sign of the first vector coordinate c_k^1 (Kisilev et al., 2000). As a result, a number of clusters corresponding to the number of the sources emerges on the hemisphere (Fig. 5).

Applying some clustering algorithm, e.g. Fuzzy C-means (FCM), it is possible to determine the cluster centroids. The coordinates of the centroids define the columns of the estimated mixing matrix, equivalently to the orientations found in the previous approach. Refinement iterations may be performed by deleting the points with low membership value and performing again FCM on the refined data set.

Lennon et al. (2001) used a dynamic vector quantization algorithm instead of clustering. This approach may be advantageous over FCM, since it does not assume an a priori knowledge of the number of sources.

It is important to note that the performance of geometric separation depends heavily on the quality of the scatter plot: the more the orientations in the scatter plot are distinguishable and clear, the higher is the accuracy in estimating the mixing matrix.

IV. SPARSE DECOMPOSITION OF IMAGES

In Section III, we showed how to separate linearly mixed images, assuming that the sources are sparse. Although one can find examples of natural signals or images that in their original space of representation, i.e. the native signal or image space, depict the property of sparseness, in most cases (including the application of separation of transmitted image from reflections superimposed by a semireflec-

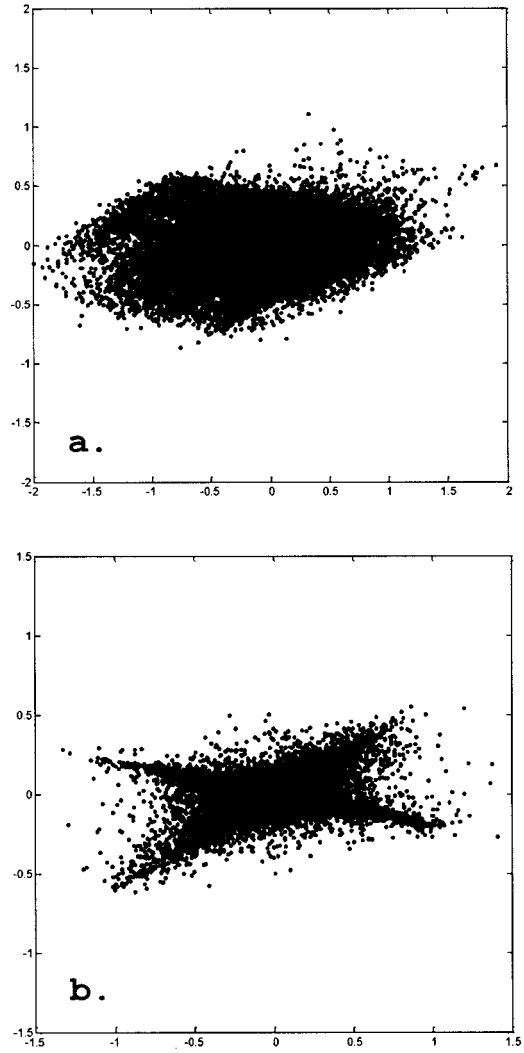


Figure 8. Scatter plot of the mixtures m_2 vs. m_1 before (a) and after (b) the sparse transformation.

10981098, 2005, 1, Downloaded from https://onlinelibrary.wiley.com/doi/10.1002/ima.20042 by CochraneAustria, Wiley Online Library on [23/09/2026]. See the Terms and Conditions (https://onlinelibrary.wiley.com/terms-and-conditions) on Wiley Online Library for rules of use; OA articles are governed by the applicable Creative Commons License

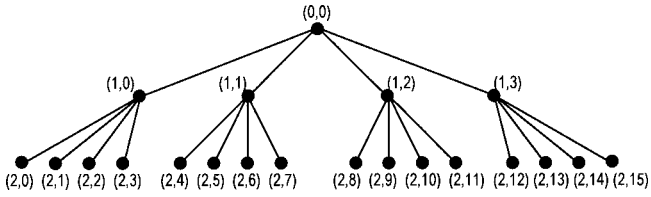


Figure 9. 2D wavelet packet tree.

tive medium), images have rather nonsparse nature. The important observations mentioned by us earlier is that such images can be sparsely represented by their projection into a proper space, i.e., there exists a linear transformation T such that

$$d_i = Ts_i \tag{7}$$

is sparse. (Note that it is not necessary to be able to restore s_i from d_i, i.e. T does not necessarily have to be invertible.) Application of the transformation to the mixtures in (3), because of the linearity of T, yields

$$Tm_i = T(a_{i1}s_1 + a_{i2}s_2) = a_{i1}d_1 + a_{i2}d_2. \tag{8}$$

Thus, the problem at hand is equivalent to separation of linearly-mixed sparse sources. This can be solved using the techniques described in Section III.

The question is then whether there exists a universal transformation that projects any given natural signal or image onto its optimal sparse representation. Unfortunately, this is not the case. Different classes of signals require their specific, optimal (in some sense), sparsification transformations (Kisilev et al., 2003). However, a wide range of transforms can result in sparse representation that permits good estimation of the mixing matrix. For example, and this is relevant to our reflection separation problem, in the case of natural images (Fig. 6), the edge distribution is usually sparse (other than in the extreme cases of densely textured image).

Thus, even such simple operations as a derivative followed by thresholding yields a sparse image (Fig. 7). The effect of this simple transformation on the potential of separation can be appreciated by comparing the scatter plots of the original mixtures (Fig. 8a) with those of the transformed mixtures (Fig. 8b). Although the two dominant orientations, corresponding to the columns of the mixing matrix, are apparent in the scatter plot of the transformed mixtures, the fuzzy cloud in the scatter plot of the original images does not permit any reasonable estimation of the mixing matrix. The reason is that the original images are endowed with nonzero pixel-value distribution all over the image space, and therefore, the probability of having a high value at a specific pixel in one image, and almost zero value in the corresponding pixel of the other image is very small.

On the other hand, since it is very unlikely that the majority of the edges of the source images will coincide, many points in the scatter plots of the mixtures are contributed by a single source only. Thus, optimality of the sparse transformation calls for the search for such a transformation that increases the proportion of those points contributed by only one of the sources.

A. Multinode Decomposition. Since there is no common sparse representation to different images, such a simple transformation as the derivative is usually data-dependent. Having this problem in mind, richer representations, that over a wide range of natural images lend themselves to relatively good sparse representations, such as the wavelet packet transform (WPT), were proposed (Kisilev et al., 2000, 2003).

The 2D WP image decomposition can be represented as the tree shown in Figure 9. The nodes of the WP tree are numbered by two indices (i, j), where $i = 0, \ldots, N$ is the depth of the level, and $j = 0, \ldots, 2^i - 1$ is the node number at the specified level (Mallat, 1998; Kisilev et al., 2000, 2003).

The task is to select only the nodes, corresponding to sparse decomposition. Kisilev et al. (2000, 2003) proposed an algorithm, according to the clustering procedure, which is first applied to each one of the nodes, but only nodes with minimal *global distortion* (i.e., the mean-squared distance of data points to the centers of the closest clusters) are then selected for further processing. A more general approach is to assign some quality factor to each node, which determines its sparseness, and then select a certain percentage of the "best" nodes in the sense of the assigned quality criterion. The choice of such a criterion is discussed in Section IV.B.

As an alternative to the WP decomposition, we propose to divide the image into blocks (possibly overlapping), compute some simple sparse transformations such as the first or the second order derivative (possibly concatenated) and only then to select the "best" blocks according to some sparseness criterion. Our observation is that most natural images have certain regions, in which edges and texture make such an approach efficient. Figure 10 depicts how the use of blocks can refine the sparseness and consequently the quality of the scatter plot in the previous example shown in Figure 6. The mixtures are partitioned into 16 blocks of equal size, and the same sparse transformation is applied to each block independently.

Clearly, the independence of the edge distributions contributed to the mixtures, from each of the sources, varies from block to block, and therefore a subset of blocks, in this example only (1,1), (1,3), and (1,4), yields the best scatter plots with two dominant orientations.

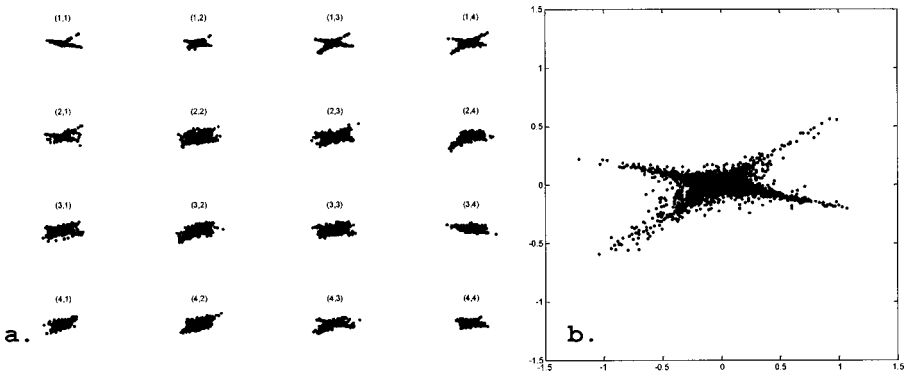


Figure 10. Sparseness refinement by image partitioning into 16 blocks. Scatter plots of the coefficients in each block, using x derivative as the sparse transformation (a) and a scatter plot resulting from merging the coefficients of blocks (1,1), (1,3), and (1,4) (b).

10981098, 2005, 1, Downloaded from https://onlinelibrary.wiley.com/doi/10.1002/ima.20042 by CochraneAustria, Wiley Online Library on [23/09/2026]. See the Terms and Conditions (https://onlinelibrary.wiley.com/terms-and-conditions) on Wiley Online Library for rules of use; OA articles are governed by the applicable Creative Commons License

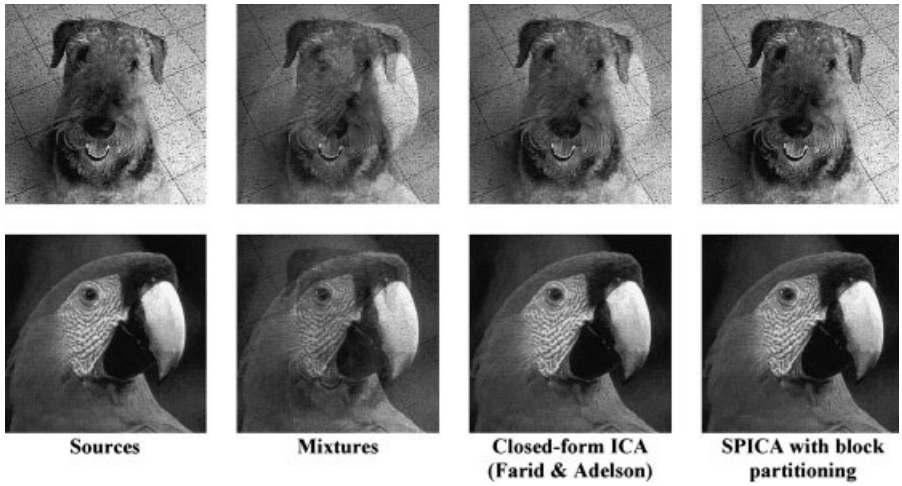


Figure 11. Separation of synthetic mixtures.

Hence, the estimation of the mixing matrix entries can be further improved by combining the data obtained from the best sets of blocks.

B. Quantitative Sparseness Criteria. Finding an adequate sparseness criterion is a crucial task for selecting the best nodes or blocks. Following Kisilev et al. (2000, 2003), one can perform the clustering procedure on each node or block and measure some distortion function of the clusters. The use of fuzzy clustering allows incorporating the membership probability as weighting of the distortion function. The main disadvantage of this approach is its high computational complexity, since it requires executing the clustering algorithm at each node. Moreover, in higher dimensions clustering usually gives poor results.

The general problem of quantitative node sparseness estimation is to find such a function $q(x)$ which, given a vector $x \in \mathbb{R}^n$, yields a large value if it is sparse or a small value if it is not sparse. One of the possibilities is to use the so-called L_0 norm (threshold), i.e., measure the number of vector coordinates, which is higher than some threshold τ:

$$q^{-1}(x) = \frac{1}{n}\sum_{k=1}^{n} \mathbf{I}(x_k \geq \tau), \tag{9}$$

where $\mathbf{I}$ is the indicator function. A natural choice of the threshold would be $\tau = \|x - \bar{x}\|_2$, where $\bar{x}$ is the mean value of x.

Yet another possible sparseness criterion is the L_p norm for $0 < p \leq 1$:

$$q^{-1}(x) = \frac{\|x\|_p}{n^{\frac{1}{p}-\frac{1}{2}} \cdot \|x\|_2} = \frac{1}{n^{\frac{1}{p}-\frac{1}{2}}} \cdot \frac{\left(\sum_{k=1}^{n} x_k^p\right)^{\frac{1}{p}}}{\left(\sum_{k=1}^{n} x_k^2\right)^{\frac{1}{2}}}. \tag{10}$$

Recent studies indicate that the L_1 norm is a more natural choice for dealing with various aspects of image quality criteria. This, normalized by the L_2 norm, as in (10), may turn out to be the best sparseness criterion. This, however, has yet to be further investigated.

V. RESULTS

The experimental results are obtained by applying the SPICA approach to polarization images obtained by simulated images as well as to images photographed in real-world conditions. The results are compared with those of Farid and Adelson (1999a,b).[1]

A. Simulated Data. In the first experiment, the mixtures were obtained by artificially mixing two source images ("Terry" and "Parrot," denoting sources A and B, respectively; left column of Fig. 11). We used two SPICA methods: WP decomposition and block partitioning with second-order Sobel numeric derivative, applied as the projection onto the space of sparse representation. The reconstruction was performed geometrically, using an angular histogram. Peak detection was performed in two stages: first, peaks' locations were estimated in a coarse histogram. Then, the coarse estimation was refined by performing peak detection in a fine histogram of the data points in a small angular spread around each of the estimated peaks.

Although one has to scrutinize the separated images in order to realize the improvement in the results obtained by the sparse representations over blocks, proposed in this study, as compared with those obtained by the application of closed-form ICA [(Farid and Adelson, 1991, 1999b); compare the left two columns of Fig. 11], the SNR values represented in Table I reveal a considerable improvement by sparse representations. It is difficult, however, to draw a clear conclusion from this simulation study about the comparison of the WP and the block partitioning. Obviously, all the localized techniques yield good results.

B. Real-world Data. To further test the performance of the three algorithms (the closed-form ICA and two versions of SPICA), we used the images of a Renoir's painting, framed behind glass, with a superimposed reflection of a mannequin ("Sheila"), photographed by Farid and Adelson through a linear polarizer at orthogonal orientations.[2] SPICA algorithms were implemented in MATLAB.[3]

The block partitioning approach is a natural way to handle the case of spatially varying mixing coefficients, which often occur in reality. A better assumption is of a locally spatially invariant system that can be dealt with by partitioning of the image into blocks. The acquired images were divided into four equally sized superblocks and the separation problem was solved in each superblock

[1] This algorithm is termed "closed-form ICA," as proposed by Prof. Hany Farid in private communications.

[2] The polarized images and the analytic ICA MATLAB code for image separation are available from http://www.cs.dartmouth.edu/~farid/research/separation.html (courtesy of Hany Farid, Dartmouth College).

[3] The SPICA MATLAB codes are available from http://visl.technion.ac.il/bron/spica.

10981098, 2005, 1, Downloaded from https://onlinelibrary.wiley.com/doi/10.1002/ima.20042 by CochraneAustria, Wiley Online Library on [23/09/2026]. See the Terms and Conditions (https://onlinelibrary.wiley.com/terms-and-conditions) on Wiley Online Library for rules of use; OA articles are governed by the applicable Creative Commons License

Table I. SNR (dB) of the reconstructed sources.

	Closed Form ICA (Farid and Adelson)	SPICA With WP Decomposition	SPICA With Block Partitioning
Estimated source A	12.18	38.58	35.83
Estimated source B	26.07	45.96	64.96

separately. The coefficients of the estimated unmixing matrix were then linearly interpolated over the entire image to produce a more accurate unmixing. Figure 12 shows the reconstruction results. The desired photographed image of Renoir's painting is recovered with high precision, without notable artifacts. The nonseparated details in the reconstructed image of the mannequin resulted from geometric distortions due to imperfections of the optical system, i.e., the optical system cannot be considered as a spatial-invariant system.

Consequently, the reconstruction of the virtual image is improved by block partitioning in two ways, first by better matching the algorithm to the nonstationarity of the sources, and second by better dealing with the spatial varying properties of the optical system. Reconstruction with WP decomposition was done under the spatial invariance assumption.

Yet another important task after performing the separation of images is to determine which of them belongs to the real object and which to the reflected one. Taking into consideration the prior knowledge of the fact that the contribution of the virtual object varies more because of polarization than the intensity of the real object (which remains almost constant), we can identify the virtual object as that corresponding to the column of the estimated mixing matrix, whose coefficients vary the most. This principle is supported by our processing of the example of the real polarized images.

VI. CONCLUSIONS

The SPICA approach can be effectively used in a wide range of scenarios wherein various mixtures of source images are available for separation of the sources. In this study, we are primarily concerned with separation of an image from virtual images superimposed on it by reflections from a semireflecting medium. The proposed novel sparse decomposition method incorporates block partitioning, suitable for nonstationary natural images, as well as for imaging systems such as polarized semireflecting media, that cannot be considered as spatial invariant systems, but can to a good approximation be dealt with as locally spatial invariant systems. Experiments conducted with simulated and photographed data show the efficiency of this approach and its advantages in the specific problem of separation of an image with superimposed reflections over previously proposed wavelet packet decomposition and closed-form ICA.

We have assumed that only two images, acquired at perpendicular polarization angles, are available. However, in its implementation to physical systems, one may extend the application to acquisition of more than two images. In this case, principal component analysis (PCA) can be used prior to the application of ICA.

Lastly, the block partitioning into fully localized subsets of data can be also useful in cases where in addition to the mixing, there is a weak effect of convolution. This combined case of mixing with convolution is, of course, much more difficult than the mixing only, and is encountered in many physical systems. However, convolution too is only an approximation of more complex action of a kernel in an integral equation that does not represent convolution. The argument of locally stationary is, however, valid in this case too. Therefore, our proposed block partitioning should improve the results regardless of the type of blind deconvolution combined with the BSS.

ACKNOWLEDGMENTS

We are indebted to Hany Farid (Dartmouth College) for kindly providing us with the polarized images, his MATLAB codes, and very valuable comments, and to Johanan Erez (VISL, Technion) for his assistance in data acquisition. This research has been supported in part by the Ollendorff Minerva Center, by the Fund for Promotion of Research at the Technion, by the Israeli Ministry of Science and by the Columbia University ONR-MURI Grant N000M-01-1-0625.

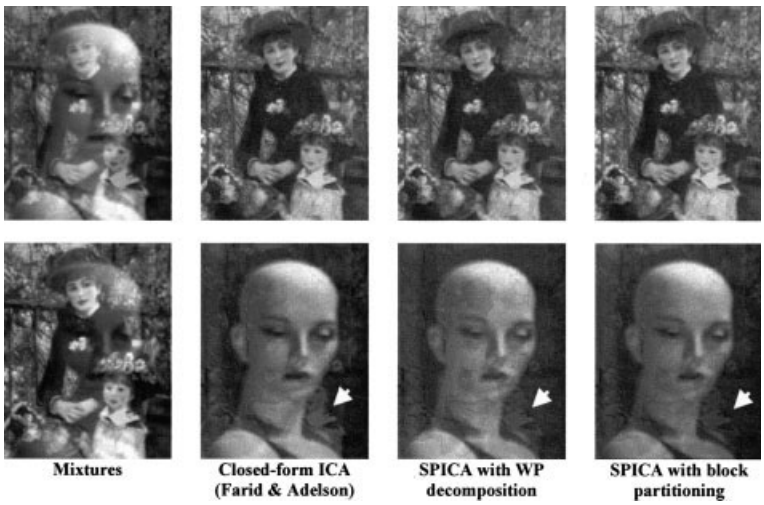


Figure 12. Separation of polarized images. Arrows point to nonseparated details in the virtual component (Sheila) reconstruction, which are significantly reduced using the blocks approach.

10981098, 2005, 1, Downloaded from https://onlinelibrary.wiley.com/doi/10.1002/ima.20042 by CochraneAustria, Wiley Online Library on [23/09/2026]. See the Terms and Conditions (https://onlinelibrary.wiley.com/terms-and-conditions) on Wiley Online Library for rules of use; OA articles are governed by the applicable Creative Commons License

REFERENCES

A.J. Bell and T.J. Sejnowski, An information-maximization approach to blind separation and blind deconvolution, Neural Comput 7(6) (1995), 1129–1159.

J.R. Bergen, P.J. Burt, R. Hingorani, and S. Peleg, Transparent motion analysis, In Proc ECCV, 1990, pp. 566–569.

T.W. Cronin, N. Shashar, and L. Wolff, Portable imaging polarimeters, In Proc ICPR, Vol- A, 1994, pp. 606–609.

H. Farid and E.H. Adelson, Separating reflections and lighting using independent component analysis, In Proc IEEE Comput Soc Conf on Computer Vision and Pattern Recognition, Fort Collins, CO, Vol. 1, 1999a, pp. 262–267.

H. Farid and E.H. Adelson, Separating reflections from images using independent component analysis, JOSA 17(9) (1999b), 2136–2145.

H. Fujikake, K. Takizawa, T. Aida, H. Kikuchi, T. Fujii, and M. Kawakita, Electrically-controllable liquid crystal polarizing filter for eliminating reflected light, Opt Rev 5 (1998), 93–98.

P. Kisilev, M. Zibulevsky, Y.Y. Zeevi, and B.A. Pearlmutter, Multiresolution framework for blind source separation, CCIT Report no. 317, Technion Press, 2000.

P. Kisilev, M. Zibulevsky, Y.Y. Zeevi, A multiscale framework for blind separation of linearly mixed signals, J Mach Learning Res 4 (2003), 1339–1373.

M. Lennon, G. Mercier, M.C. Mouchot, and L. Hubert-Moy, Spectral unmixing of hyperspectral images with the independent component analysis and wavelet packets, In Proc IGARSS, 2001.

S. Mallat, A wavelet tour of signal processing, Academic Press, New York, 1998.

K.S. Nayar, X.S. Fang, and T. Boult, Separation of reflection components using color and polarization, Int J Comput Vis 21 (1997), 163–186.

Y.Y. Schechner, J. Shamir, and N. Kiryati, Polarization-based decorrelation of transparent layers: the inclination angle of an invisible surface, In Proc Int Conf on Computer Vision, 1999, pp. 814–819.

Y.Y. Schechner, J. Shamir, and N. Kiryati, Polarization and statistical analysis of scenes containing a semireflector, JOSA A 17(2) (2000), 276–284.

M. Shizawa, On visual ambiguities due to transparency in motion and stereo, In Proc ECCV, 1992, pp. 411–419.

M. Zibulevsky and B.A. Pearlmutter, Blind source separation by sparse decomposition, Neural Comput 13(4) (2001), 683–882.

M. Zibulevsky, P. Kisilev, Y.Y. Zeevi, and B.A. Pearlmutter, Blind source separation via multinode sparse representation, In NIPS-2001, Morgan Kaufmann, San Mateo, CA, 2001, pp. 185–191.

10981098, 2005, 1, Downloaded from https://onlinelibrary.wiley.com/doi/10.1002/ima.20042 by CochraneAustria, Wiley Online Library on [23/09/2026]. See the Terms and Conditions (https://onlinelibrary.wiley.com/terms-and-conditions) on Wiley Online Library for rules of use; OA articles are governed by the applicable Creative Commons License